Journal of Advanced Ceramics

Volume 9 | Issue 5 Article 7

2020

Effect of octahedron tilt on the structure and magnetic properties of bismuth ferrite

Yang HONG
School of Physics, Harbin Institute of Technology, Harbin 150001, China

Jun LI
School of Physics, Harbin Institute of Technology, Harbin 150001, China

Han BAI
School of Physics, Harbin Institute of Technology, Harbin 150001, China

Zhenjia SONG
School of Physics, Harbin Institute of Technology, Harbin 150001, China

Ming WANG
School of Physics, Harbin Institute of Technology, Harbin 150001, China

See next page for additional authors

Effect of octahedron tilt on the structure and magnetic properties of bismuth ferrite

Authors

Yang HONG, Jun LI, Han BAI, Zhenjia SONG, Ming WANG, and Zhongxiang ZHOU

Journal of Advanced Ceramics
2020, **9**(5): 641–646
https://doi.org/10.1007/s40145-020-0398-1

ISSN 2226-4108
CN 10-1154/TQ

Rapid Communication

Effect of octahedron tilt on the structure and magnetic properties of bismuth ferrite

Yang HONG, Jun LI*, Han BAI, Zhenjia SONG, Ming WANG, Zhongxiang ZHOU*

School of Physics, *Harbin Institute of Technology*, *Harbin 150001*, *China*

Received: April 22, 2020; Revised: May 31, 2020; Accepted: June 18, 2020

Abstract: Multiferroic $BiFeO_3$-based ceramics were synthesized using the rapid liquid-phase sintering method. The rare-earth ion (Sm^{3+}, Gd^{3+}, Y^{3+}) doping causes structural distortion without changing the intrinsic rhombohedral perovskite structure. Raman analysis shows that the effect of doping on E modes is greater than A_1 modes, and the microstructure of FeO_6 octahedron can be regulated by ion doping. A-site trivalent ion doped ceramics exhibit improved magnetism compared with pure $BiFeO_3$ ceramic, which originated from the suppressed spiral spin structure of Fe ions. The tilt of FeO_6 octahedron as a typical structure instability causes the anomalous change of the imaginary part of permittivity at high frequency, and doped ceramics exhibit natural resonance around 16–17 GHz.

Keywords: bismuth ferrite ($BiFeO_3$); magnetism; octahedron tilt; Raman spectrum; electromagnetic characteristics

1 Introduction

Multiferroic materials are one of the most studied materials in recent years due to their unique properties, which exhibit more than two ferroic orders (such as ferroelectricity (T_C), ferromagnetism (T_N), ferroelastic, etc.). More than two orders can be coupled under certain conditions, exhibiting remarkable physical properties and excellent application potential [1–4]. Multiferroic materials are not only helpful for the applications but also provide a platform for exploring interesting effects like magnetoelectric effect, piezoelectric effect, etc. [5,6].

Among various known multiferroic materials, bismuth ferrite ($BiFeO_3$, abbreviated as BFO) is a widely investigated multiferroic material, in which $T_C \approx 1100$ K and $T_N \approx 640$ K coexist at room temperature [7,8]. The crystallographic structure of BFO is rhombohedral distorted perovskite structure with the space group $R3c$. The unit cell has a lattice parameter of $a = 3.965$ Å and a rhombohedral angle of ~89.3°–89.48°, and the oxygen octahedron is distorted with the minimum and the maximum O–O distances of 2.710 and 3.015 Å, respectively, and rotated by about 13.8° around the [111] axis [9]. BFO is classified as a G-type antiferromagnet below T_N at the magnetic point of view; the combined action of exchange and spin–orbit interactions produce spin canting away from perfect antiferromagnetic ordering. The canted spin structure exhibits a space-modulated spiral structure (SMSS) with a period length of 62 nm, thereby resulting in a helimagnetic structure and a vanishing magnetization in the bulk [10,11].

The SMSS ordering in BFO is stable, and it persists when the temperature varies from 4 K to the Neel

* Corresponding authors.
E-mail: J. Li, lijuna@hit.edu.cn;
Z. Zhou, zhouzx@hit.edu.cn

temperature [12]. The modification of the spin structure is the key issue for the realization of $BiFeO_3$-based materials, and many attempts to add ferromagnetic properties to the BFO compounds by A- or B-site substitutions were made. Neutron diffraction studies on $Bi_{1-x}La_xFeO_3$ show that the SMSS modulation period in BFO grows with La, and researchers have found that the leakage current of BFO can be reduced by substituting appropriate element [13]. To improve the electrical and magnetic properties of the BFO, several research groups have attempted to modify with trivalent ions of Nd^{3+}, Dy^{3+}, or Pr^{3+} at the A-site of BFO [14–17]. Jena *et al*. [18] found that the spin-coated Y-doped BFO film exhibits low field saturation magnetization by suppressing the spiral spin modulated periodicity due to FeO_6 octahedral distortion.

In present study, we studied structure, magnetic properties, and microwave electromagnetic parameters of $BiFeO_3$-based ceramics. A-site trivalent ion doping tilted the FeO_6 octahedron in the lattice and changed the space-modulated spiral structure, leading to the improved ferromagnetism of ceramics. Doped samples exhibited enhanced permittivity accompanied natural resonance around 16–17 GHz, and the detailed mechanism has been explained with dielectric loss and defects changed.

2 Experimental

Polycrystalline BFO and $Bi_{0.95}M_{0.05}FeO_3$ (M = Sm, Gd, and Y, abbreviated as BSFO, BGFO, and BYFO, respectively) samples were prepared by the rapid liquid-phase sintering method. Stoichiometric ratios of Bi_2O_3, Fe_2O_3, Sm_2O_3, Gd_2O_3, and Y_2O_3 were mixed with agate balls for 24 h using alcohol as the solvent. Each component has an increase of 2.5% Bi_2O_3 on the base of the stoichiometric ratio, considering the volatilization characteristic of Bi_2O_3. The powders were pressed into pellets of 8 mm in diameter under 500 MPa rapidly sintered in air at 800 ℃ for 20 min, and then took a rapid air quenching process.

The phase composition and crystalline structure of the samples were analyzed using X-ray diffraction (XRD, Panalytical X'PERT PRO MPD, with Cu Kα radiation). Morphologies were examined using field emission scanning electron microscopy (SEM, ZEISS Merlin Compact). Raman measurement was performed using a laser confocal Raman spectrometer (inVia-Reflex, Renishaw). The magnetic properties were investigated by a vibrating sample magnetometer (VSM). The electromagnetic parameters were measured from 2 to 18 GHz with a vector network analyzer (Keysight Technologies N5234A).

3 Results and discussion

In order to evaluate the phase formation and crystallinity of the samples, an XRD study was performed, and the effect of the substitution of doped ions for Bi^{3+} ion on the structure of $BiFeO_3$ was investigated by Rietveld refinement, which was performed by using the GSAS program. Figure 1(a) shows the XRD patterns and the refinement curves of the as-prepared samples, and Fig. 1(b) provides the partial enlarged diffraction peaks around 32°. Yobs and Ycal represent the intensity of the experimental diffraction peak and the fitted diffraction peak, and Ydif is the difference between Yobs and Ycal. All the exhibited peaks of four samples can be well indexed by $BiFeO_3$ (ICDD-PDF No. 71-2494) with a rhombohedral perovskite structure. The corresponding lattice parameters and fitting factors are listed in Table 1, ion introduction plays a significant effect on the crystal structure. Since the radius of the doped ions is smaller than that of the bismuth ion (eight-coordination ionic radius: $r(Bi^{3+})$ = 0.117 nm, $r(Sm^{3+})$ = 0.1079 nm, $r(Gd^{3+})$ = 0.1053 nm, $r(Y^{3+})$ = 0.1019 nm), the unit cell volume shrinks after doping. Figure 1(b) also exhibits the change of the crystal structure according to the law of Bragg diffraction, the diffraction peaks shift to the high angle as the radius of doped ions decreases. In addition, affected by the change of ion radius in the sublattice, the state of the local electronic cloud changed, so the bond length (Fe–O) and the bond angle (Fe–O–Fe) have changed in the FeO_6 octahedron, and the FeO_6 octahedron distorted. The smaller average

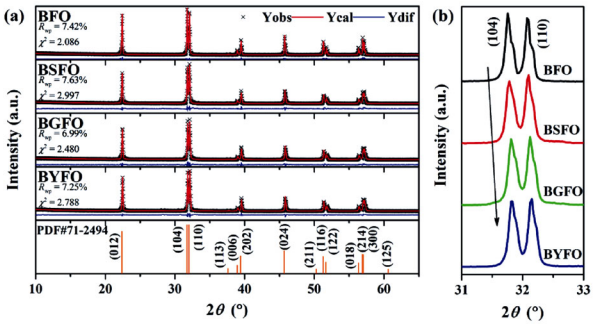

Fig. 1 (a) Rietveld-refined XRD patterns and (b) the partial enlarged XRD peaks of BFO, BSFO, BGFO, and BYFO samples.

Table 1 Refined lattice parameters and structure fitting factors

Parameter	BFO	BSFO	BGFO	BYFO
a (Å)	5.5795	5.5798	5.5788	5.5794
c (Å)	13.8709	13.8623	13.8609	13.8687
V (Å^3)	373.960	373.767	373.594	373.893
Fe, z	0.2222	0.2456	0.2707	0.2316
O, x	0.4520	0.4360	0.4440	0.4277
O, y	0.0227	0.0003	0.0092	–0.0130
O, z	0.9554	0.9807	1.0020	0.9995
Fe–O(1) bond length (Å)	2.071	2.138	2.137	2.122
Fe–O(2) bond length (Å)	1.980	1.905	1.912	1.939
Fe–O–Fe bond angle (°)	165.7	170.3	166.5	166.5
R_{wp}	7.42%	7.63%	6.99%	7.25%
R_p	5.80%	5.87%	5.51%	5.47%
χ^2	2.086	2.997	2.480	2.788

ionic radius of A-site results in a larger distortion of the lattice.

The angle of rotation of oxygen octahedron is a typical structural parameter of BFO, which changes monotonously with the tolerance factor. Therefore, the distortion of oxygen octahedron can be qualitatively analyzed through the change of tolerance factor. For cubic perovskite with standard matching ions, this rotation angle is zero. However, in BFO rhombohedral perovskite system, the rotation angle is nonzero for the influence of overlap between the electronic clouds of ions.

In the doped system of perovskite structure compounds, the tolerance factor, defined as $\tau = (r_A + r_O)/(\sqrt{2}(r_B + r_O))$, is usually used to depict the stable extent of the structure. r_A, r_B, and r_O stand for the ionic radius of A-site, B-site, and O-site in the ABO_3, respectively [19, 20]. The τ is 0.8887 for the pure BFO, and it is 0.8871, 0.8866, and 0.8860 for BSFO, BGFO, and BYFO, respectively. It can be seen that the structure of the four components is relatively stable. The smaller the tolerance factor, the more severe the bending between the oxygen octahedrons. The smaller A-site ions can not fill the space fully leading to the distorted octahedron, shrinking the unit cell space. The octahedral tilt is ~11°–14° along the [111] triple-axis and the related Fe–O–Fe band angle is 154°–156° [20].

SEM technology was used in pure and doped BFO samples, as shown in Fig. 2. All the samples exhibit distinct morphologies and boundaries, and a certain amount of pores exist in the ceramics. In order to avoid heterogeneous phases during sintering, rapid liquid-phase sintering and air quenching were adopted, which have caused a change in the porosity of the ceramics. The grain size of pure BFO was found to be 1–3 μm; with the introduction of doped ions, the average grain sizes of doped ceramics are smaller than that of BFO, which are around 0.5–1 μm. The difference in the ionic radius of the A-site will cause the shrinkage of unit cells which will hinder the nucleation of crystallites, and the grain sizes are smaller in the submicron scale.

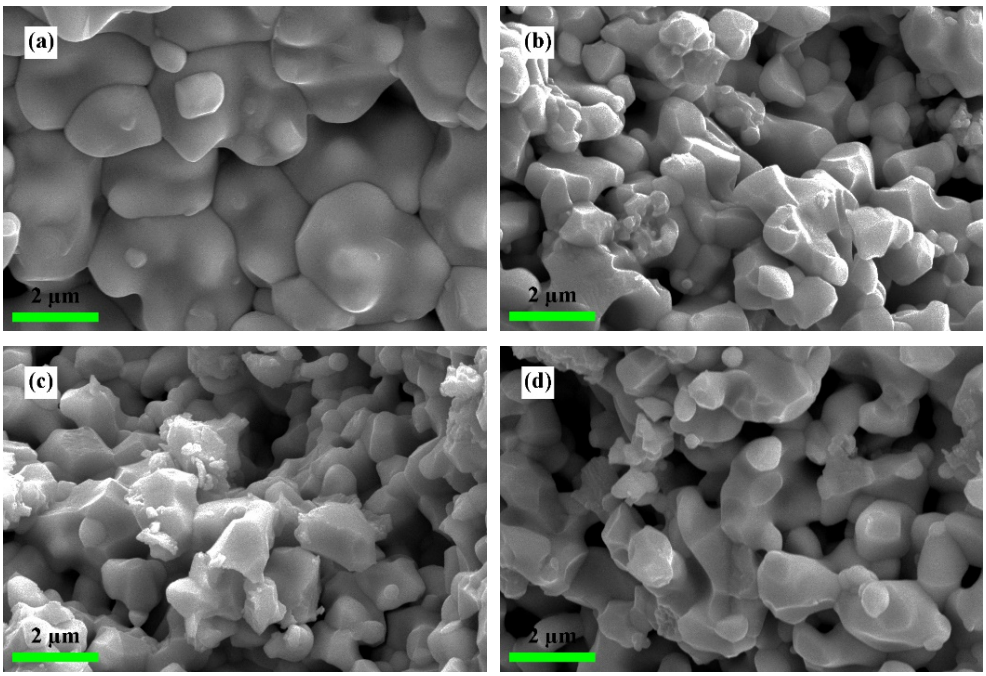

Fig. 2 SEM micrographs of as-prepared ceramics: (a) BFO, (b) BSFO, (c) BGFO, and (d) BYFO.

The crystal structure of BFO is a distorted rhombohedral perovskite at room temperature, which belongs to space group *R*3*c*. According to the group theory, the multiferroic BFO exhibits 13 optical phonon modes, expressed by the equation as

$$\Gamma_{\text{Rhombohedral},R3c} = 4A_1 + 9E \quad (1)$$

where the A_1 mode polarized along and the doubly degenerate E modes polarized in the *x*–*y* plane are both Raman and IR active. The peaks, which represent the Raman modes, were obtained by the Raman spectra and decomposed into individual components, as shown in Fig. 3. In our polycrystalline ceramics, all the 13 Raman active modes were observed, which matched well with the above structure. Bi atoms participate in low-frequency modes below A_1(TO1), whereas O atoms dominate in modes above E(TO4). Fe atoms are involved mainly in modes between E(TO2) and E(TO4), but also contribute to the development of some higher-wavenumber modes.

We observed all Raman modes of the rhombohedral structure of $BiFeO_3$ predicted by theory from the spectrum, and labeled them in Fig. 3. Table 2 exhibits the comparison of the Raman mode positions after being deconvoluted of different component samples. By comparing Raman shifts of different modes, it is found that the doping has a certain effect on the E modes, but has little effect on the A_1 modes.

Figure 4 exhibits the *M*–*H* hysteresis loops for pure and doped BFO ceramics under the maximum applied field of 15 kOe at room temperature. BFO possesses a space-modulated spiral structure superimposed on the G-type antiferromagnetic ordering with a period of 62 nm [21]. The behavior of the magnetization goes up with the increasing of the magnetic field in a linear relation, indicating that the BFO has an antiferromagnetic nature due to the spin cycloid and the sloping angle of Fe–O–Fe [22]. Table 3 shows the remanent magnetization (M_r) and coercivity (H_c) of pure and doped BFO ceramics. The M_r of the Sm, Gd, and Y doped samples has an obvious upgrade comparing with the undoped BFO. Trivalent ion doping can change the lattice structure and restrain the intrinsic space-modulated spiral structure of BFO; as a result, the magnetic performance is improved. In the FeO_6 octahedron, doping will lead to the variation of the bond distance (Fe–O) and bond angle (Fe–O–Fe), which indicates that the octahedron has been distorted, and the potential magnetization can be released [23]. The results indicate that the rare earth ion doping can effectively improve the magnetic properties of BFO at room

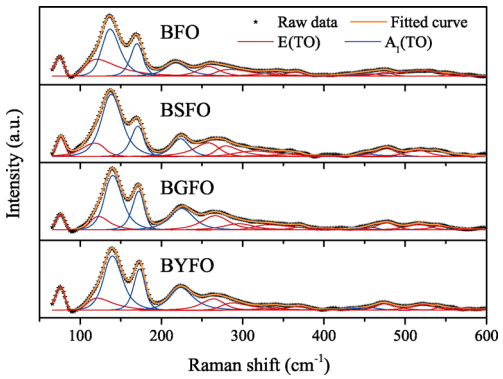

Fig. 3 Deconvoluted Raman spectra of BFO, BSFO, BGFO, and BYFO ceramics.

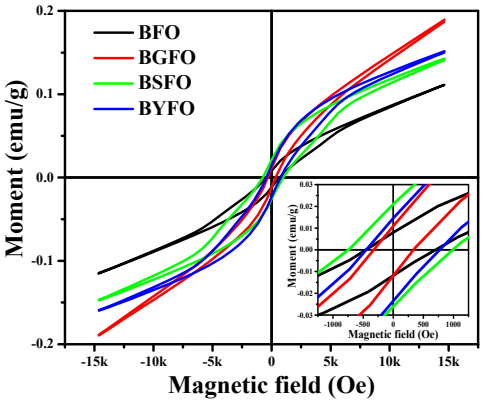

Fig. 4 *M*–*H* hysteresis loops for pure and doped BFO ceramics, and the inset depicts partial enlarged curves.

Table 2 Comparison of the Raman mode positions of different component samples

Raman mode	BFO	BSFO	BGFO	BYFO
A_1(TO1)	137	138	140	140
A_1(TO2)	170	171	172	173
A_1(TO3)	218	224	225	224
A_1(TO4)	453	450	450	456
E(TO1)	75	76	76	76
E(TO2)	121	118	123	121
E(TO3)	258	258	266	264
E(TO4)	284	279	295	288
E(TO5)	340	314	333	338
E(TO6)	366	360	370	370
E(TO7)	476	477	477	475
E(TO8)	523	516	517	522
E(TO9)	557	540	571	543

Table 3 Detailed magnetic parameters of pure and doped BFO ceramics

Parameter	BFO	BSFO	BGFO	BYFO
M_r (emu/g)	0.009	0.023	0.011	0.019
H_c (Oe)	579	866	331	611

temperature. $BiFeO_3$ is a typical weak magnetic material with the unique periodic spiral spin structure. The main reason for the unsaturated hysteresis loop is that the periodic spiral spin structure suppresses the spin magnetic moment of each Fe ion, especially in ceramic-based materials with larger grains. The periodic spiral spin structure will superimpose a net magnetic moment, which cannot opportunely respond with the change of the external magnetic field since the spin magnetic moment of each Fe ion is restricted.

In order to explore the microwave electromagnetic properties of samples, the air-line method was employed to measure the complex permittivity and complex permeability within the 2–18 GHz, as shown in Figs. 5(a) and 5(b). According to Fig. 5, the real part of permittivity is improved for doped components, and accompanied by a certain resonance at 16–17 GHz. Among the samples, BGFO shows better dielectric loss. Due to the use of a rapid liquid-phase sintering method, the complex permittivity for each component is at a low level. The leakage current caused by oxygen vacancy is widely considered to be a major influential factor in the dielectric loss for BFO in the microwave band [24,25], and we suppose that other defects

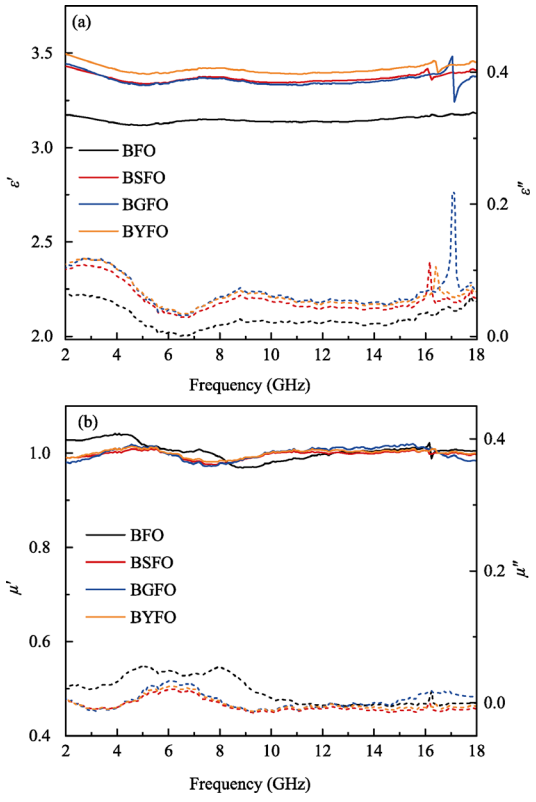

Fig. 5 (a) Real and imaginary parts of permittivity and (b) real and imaginary parts of permeability of BFO, BSFO, BGFO, and BYFO, respectively.

generated during the preparation process will also have a negligible effect on the dielectric properties of ceramics. The real part of complex permeability μ' is around 1, and the imaginary part (μ'') is close to zero. The feature of the complex permeability for ceramics exhibits the inherent weak ferromagnetism of samples, which is consistent with previous magnetic analysis.

4 Conclusions

A series of doped BFO ceramics were successfully synthesized by the rapid liquid-phase sintering method. The participation of rare-earth ions modulated the spatial structure of BFO to a certain extent, and tilted the FeO_6 octahedron. The space-modulated spiral structure of BFO was further suppressed due to the minor change in a periodic structure, which is originated from the tilting of oxygen octahedron by the doping of trivalent ions, improved ferromagnetism of doped ceramics. Moreover, doped ceramics exhibit enhanced permittivity accompanied natural resonance around 16–17 GHz, and the obtained results provide a feasible route to further regulate the microwave electromagnetic performance of bismuth ferrite-based ceramics.

Acknowledgements

This study was supported by the National Natural Science Foundation of China (51502054), the Postdoctoral Science Foundation of China (2014M551236), and the Postdoctoral Science Foundation of Heilongjiang Province (LBH-Z14083).

References

[1] Chen ZH, Luo ZL, Huang CW, *et al*. Low-symmetry monoclinic phases and polarization rotation path mediated by epitaxial strain in multiferroic $BiFeO_3$ thin films. *Adv Funct Mater* 2011, **21**: 133–138.

[2] Wu JG, Fan Z, Xiao DQ, *et al*. Multiferroic bismuth ferrite-based materials for multifunctional applications: Ceramic bulks, thin films and nanostructures. *Prog Mater Sci* 2016, **84**: 335–402.

[3] Wang SS, Wu Z, Chen J, *et al*. Lead-free sodium niobate nanowires with strong piezo-catalysis for dye wastewater degradation. *Ceram Int* 2019, **45**: 11703–11708.

[4] Pan H, Li F, Liu Y, *et al*. Ultrahigh-energy density lead-free dielectric films via polymorphic nanodomain design.

Science 2019, **365**: 578–582.
[5] Ismail M, Wu Z, Zhang LH, *et al*. High-efficient synergy of piezocatalysis and photocatalysis in bismuth oxychloride nanomaterial for dye decomposition. *Chemosphere* 2019, **228**: 212–218.
[6] Ma JP, Ren J, Jia YM, *et al*. High efficiency bi-harvesting light/vibration energy using piezoelectric zinc oxide nanorods for dye decomposition. *Nano Energy* 2019, **62**: 376–383.
[7] Hong Y, Li J, Bai H, *et al*. Role of finite-size effect in $BiFeO_3$ nanoparticles to enhance ferromagnetism and microwave absorption. *Appl Phys Lett* 2020, **116**: 013103.
[8] Shirolkar MM, Dong XL, Li JN, *et al*. Observation of nanotwinning and room temperature ferromagnetism in sub-5 nm $BiFeO_3$ nanoparticles: A combined experimental and theoretical study. *Phys Chem Chem Phys* 2016, **18**: 25409–25420.
[9] Kubel F, Schmid H. Structure of a ferroelectric and ferroelastic monodomain crystal of the perovskite $BiFeO_3$. *Acta Crystallogr Sect B* 1990, **46**: 698–702.
[10] Wang J. Epitaxial $BiFeO_3$ multiferroic thin film heterostructures. *Science* 2003, **299**: 1719–1722.
[11] Sosnowska I, Azuma M, Przeniosło R, *et al*. Crystal and magnetic structure in Co-substituted $BiFeO_3$. *Inorg Chem* 2013, **52**: 13269–13277.
[12] Delaire O, Stone MB, Ma J, *et al*. Anharmonic phonons and magnons in $BiFeO_3$. *Phys Rev B* 2012, **85**: 064405.
[13] Sosnowska I, Loewenhaupt M, David WIF, *et al*. Searching for the magnetic spiral arrangement in $Bi_{0.7}La_{0.3}FeO_3$. *Mater Sci Forum* 1993, **133**–**136**: 683–686.
[14] Tu CS, Chen PY, Chen CS, *et al*. Tailoring microstructure and photovoltaic effect in multiferroic Nd-substituted $BiFeO_3$ ceramics by processing atmosphere modification. *J Eur Ceram Soc* 2018, **38**: 1389–1398.
[15] Pattanayak S, Choudhary RNP, Das PR, *et al*. Effect of Dy-substitution on structural, electrical and magnetic properties of multiferroic $BiFeO_3$ ceramics. *Ceram Int* 2014, **40**: 7983–7991.
[16] Wang N, Li Y, Wang FL, *et al*. Structure, magnetic and ferroelectric properties of Sm and Sc doped $BiFeO_3$ polycrystalline ceramics. *J Alloys Compd* 2019, **789**: 894–903.
[17] Xu XL, Xiao LB, Jia YM, *et al*. Pyro-catalytic hydrogen evolution by $Ba_{0.7}Sr_{0.3}TiO_3$ nanoparticles: Harvesting cold–hot alternation energy near room-temperature. *Energy Environ Sci* 2018, **11**: 2198–2207.
[18] Jena AK, Satapathy S, Mohanty J. Magnetic properties and oxygen migration induced resistive switching effect in Y substituted multiferroic bismuth ferrite. *Phys Chem Chem Phys* 2019, **21**: 15854–15860.
[19] Yang CH, Kan D, Takeuchi I, *et al*. Doping $BiFeO_3$: Approaches and enhanced functionality. *Phys Chem Chem Phys* 2012, **14**: 15953–15962.
[20] Wei J, Wu CF, Yang TT, *et al*. Temperature-driven multiferroic phase transitions and structural instability evolution in lanthanum-substituted bismuth ferrite. *J Phys Chem C* 2019, **123**: 4457–4468.
[21] Catalan G, Scott JF. Physics and applications of bismuth ferrite. *Adv Mater* 2009, **21**: 2463–2485.
[22] Lennox RC, Price MC, Jamieson W, *et al*. Strain driven structural phase transformations in dysprosium doped $BiFeO_3$ ceramics. *J Mater Chem C* 2014, **2**: 3345–3360.
[23] Dutta DP, Mandal BP, Mukadam MD, *et al*. Improved magnetic and ferroelectric properties of Sc and Ti codoped multiferroic nano $BiFeO_3$ prepared via sonochemical synthesis. *Dalton Trans* 2014, **43**: 7838.
[24] Sharma P, Satapathy S, Varshney D, *et al*. Effect of sintering temperature on structure and multiferroic properties of $Bi_{0.825}Sm_{0.175}FeO_3$ ceramics. *Mater Chem Phys* 2015, **162**: 469–476.
[25] Liu X, Wang LS, Ma YT, *et al*. Enhanced microwave absorption properties by tuning cation deficiency of perovskite oxides of two-dimensional $LaFeO_3$/C composite in X-band. *ACS Appl Mater Interfaces* 2017, **9**: 7601–7610.
[26] Yuan J, Hou ZL, Yang HJ, *et al*. High dielectric loss and microwave absorption behavior of multiferroic $BiFeO_3$ ceramic. *Ceram Int* 2013, **39**: 7241–7246.